HEFAT2010
7th International Conference on Heat Transfer, Fluid Mechanics and Thermodynamics
19-21 July 2010
Antalya, Turkey

MODELING AND SIMULATION OF A LARGE-SCALE METAL-HYDRIDE STORAGE TANK ON THE BASIS OF SODIUM ALANATE

Ch. Na Ranong*[1], J. Hapke[1], M. Höhne[1], G. Fieg[1] and J. Bellosta von Colbe[2]
*Author for correspondence
[1]Institute of Process and Plant Engineering,
Hamburg University of Technology,
D-21071 Hamburg
phone: +49 40 42878 3148, fax: +49 40 42878 2992
E-mail: c.naranong@tu-harburg.de

[2]Institute of Materials Research,
GKSS Research Centre,
D-21502 Geesthacht

ABSTRACT

In the framework of the European Union project STORHY (Hydrogen Storage for Automotive Applications) a metal-hydride storage tank with 8 kg sodium alanate has been recently built. A main challenge is the heat management of the system caused by the high energy flows during the exothermic loading of the hydride storage tank in relatively short periods. For the prediction of operation in passenger cars a model for the thermal behavior of this storage tank has been developed which takes into account the thermodynamic properties of the sodium alanate material as well as the reaction kinetics. These data have been derived by experiments and inserted into the balance equations. For different operating conditions an analysis has been performed. This refers to three different flow rates of the heat transfer fluid (trade name Marlotherm X). At the beginning the storage tank does not contain any hydrogen. The initial temperature of the system is 100 °C and the absorption pressure 100 bar. The inlet temperature of the heat transfer fluid has been set to 100 °C. The heat transfer coefficient between the storage elements and the heat transfer fluid depends on its flow rate. The transient absorption behavior of the storage tank has been calculated. Furthermore, it has been investigated to which extent the loading behavior can be accelerated by enhanced heat transfer due to insertion of flow baffles on the side of the heat transfer fluid. By simulation the potential for optimization of the tank geometry and the flow conditions for loading and deloading can be determined.

INTRODUCTION

The objective of EU project STORHY [1] has been the evaluation of gaseous, liquid and solid state hydrogen storage tanks for automotive applications. A crucial point with metal hydride storage tanks is the operation behavior due to high energy flows during the exothermic loading in relatively short periods. For the thorough analysis of this problem a prototype hydrogen storage tank on the basis of sodium alanate, filled with 8 kg of this hydride material, has been built. In this paper the operation behavior is predicted and discussed applying modeling and simulation.

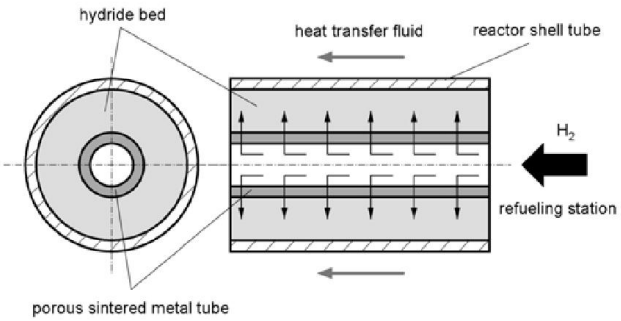

Figure 1 Working principle of a tubular reactor

Figure 1 shows the working principle of a hydride storage tank exemplarily for a tubular reactor. It consists of three components: reactor shell tube, hydride bed and porous sintered metal tube. During loading by the refueling station, hydrogen flows through the sintered metal tube into the hydride bed. The sintered metal tube is permeable for hydrogen but not for the hydride material. It fulfills the function of hydrogen distribution inside the reactor and works as a filter preventing emission of hydride material out of the storage tank into the surroundings. The hydride bed absorbs hydrogen in an exothermic chemical

reaction. The released energy is transferred through the reactor shell tube to the heat transfer fluid. The reactor shell tube separates hydride bed and heat transfer fluid. For operation of a fuel cell, the fully loaded tubular reactor is heated by the heat transfer fluid. In the hydride bed the endothermic desorption reaction takes place. The released hydrogen flows from the hydride bed through the porous sintered metal tube to the fuel cell.

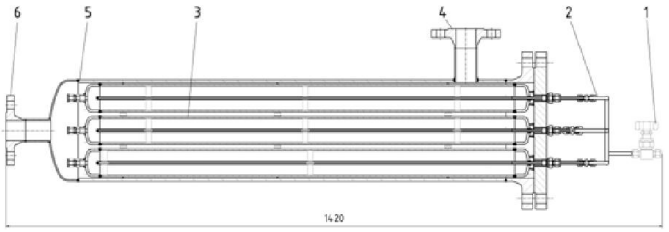

Figure 2 Prototype design: (1) hydrogen valve, (2) hydrogen supply spiral, (3) reactor element, (4) inlet nozzle of the heat transfer fluid, (5) shell, (6) outlet nozzle of the heat transfer fluid, (7) porous sintered metal tube, (8) support of sintered metal tube, (9) reactor element shell, (10) gastight hydrogen supply tube

The favored concept for manufacture is a tube bundle of reactor elements according to Figure 1 which are connected in parallel on the hydrogen side. The optimum geometry of the tubular reactor elements has been found by simulation [2]. The tube bundle of the longitudinal flow shell-and-tube apparatus (Figure 2) consists of seven reactor elements. The sectional view in Figure 2 shows three of seven reactor elements. The heat transfer fluid has one pass on the shell side. During loading hydrogen enters the storage tank through the valve (1). The spiral manifold (2) supplies the hydrogen to the reactor elements (3) which are connected in parallel. The heat transfer fluid enters the storage tank through the inlet nozzle (4) of the shell (5). It flows longitudinally over the reactor elements (3) and leaves through the outlet nozzle (6). As heat transfer fluid Marlotherm X [3] is chosen for safety reasons. In contrast to water it does not chemically react with the active material [1]. The design is certified according to EC pressure equipment directive 97/23/EC. The conformity assessment procedure of category IV, module G (EC unit verification) has been applied. The calculation code is AD 2000 (calculation pressure: 150 bar, calculation temperature: 300 °C) [4]. All pressure parts are manufactured from the material 1.4571. This austenitic steel is high-pressure hydrogen resistant.

NOMENCLATURE

A_0	[m^2]	surface area of reactor element shell tubes
$A_{q,HTF}$	[m^2]	flow cross-sectional area of heat transfer fluid
c_p	[J/(kg K)]	specific isobaric heat capacity
ΔH_R	[J/mol]	enthalpy of reaction per mole of hydrogen
h	[W/(m^2 K)]	heat transfer coefficient
k	[W/(m K)]	heat conductivity of solids
k_{eff}	[W/(m K)]	effective heat conductivity of porous medium
L	[m]	length of reactor element
M_{H_2}	[kg/mol]	molecular mass of hydrogen
n	[m]	normal outward spatial coordinate
n_v	[m]	normal spatial coordinate in the flow direction
$\vec{n}$	[-]	outward normal unit vector
p	[bar]	pressure
p_0	[bar]	reference pressure, p_0 = 1 bar
T	[K]	temperature
t	[s]	time coordinate
$\vec{u}_{HTF}$	[m/s]	mean flow velocity of heat transfer fluid
$\vec{v}_f$	[m/s]	flow velocity vector of hydrogen
w	[-]	hydrogen content
X	[-]	normalized hydrogen content
X_β	[-]	degree of reaction of step β
X_γ	[-]	degree of reaction of step γ

Greek letters

ε	[-]	porosity
η	[kg/(m s)]	dynamic viscosity
κ	[m^2]	permeability
ρ	[kg/m^3]	density
ϑ	[°C]	temperature
ϕ	[W/m^3]	source term of energy equation
ψ	[kg/(m^3 s)]	source term of mass balance equation

Super- and subscripts

b	hydride bed
f	fluid
HTF	heat transfer fluid Marlotherm X
max	maximum
St	solid material of porous sintered metal tube
s	solid material of porous hydride bed
t	sintered metal tube
W	reactor shell tube
β	reaction step
γ	reaction step
0	initial

Accent

.	rate of change

Abbreviations

EU	European Union
STORHY	Hydrogen Storage for Automotive Applications

MODELING OF METAL HYDRIDE STORAGE TANKS

To predict the operation behavior of a metal hydride storage tank a mathematical tool is required, which is able to pre-calculate the absorbed mass of hydrogen as a function of time for arbitrary operating conditions. This is achieved by modeling and simulation. Each component of the storage tank is described by balance equations for mass, momentum and energy and the corresponding boundary and initial conditions. The model is implemented into the software package COMSOL [5]. The coupled partial differential equations are solved numerically with the finite element method [5]. As result, for each point in time and space the following quantities are known: hydrogen content, temperature, pressure, flow velocity of hydrogen and the degrees of reaction between hydrogen and hydride material.

Balance equations

A tubular reactor (Figure 3) consists of three components which are modeled as three different calculation domains: sintered metal tube (G1), hydride bed (G2) and reactor element shell tube (G3). Hydride bed and the sintered metal tube are porous media [6].

Porous medium "sintered metal tube" (*t*) consists of solid material (*St*) and fluid material (*f*). Solid material of the sintered metal tube is steel 1.4404. The fluid material is pure gaseous hydrogen.

Mass balance equation of hydrogen for the sintered metal tube (G1 in Figure 3):

$$\varepsilon_t \frac{\partial \rho_f}{\partial t} + \nabla \cdot \left(\rho_f \vec{v}_{f,t} \right) = 0 \tag{1}$$

For convection in porous media the momentum balance equation is replaced by Darcy's Law, Eq. (2), yielding the flow velocity vector required in Eqs. (1) and (3).

$$\vec{v}_{f,t} = -\frac{\kappa_t}{\eta_f} \nabla p_t \tag{2}$$

Energy equation of the sintered metal tube (G1 in Figure 3):

$$\left[(1-\varepsilon_t) \cdot \left(\rho c_p \right)_{St} + \varepsilon_t \left(\rho c_p \right)_f \right] \frac{\partial T_t}{\partial t} + \left(\rho c_p \right)_f \vec{v}_{f,t} \nabla T_t = \nabla \cdot \left(k_{eff,t} \nabla T_t \right) \tag{3}$$

Porous medium "hydride bed" (*b*) consists of solid material (*s*) and fluid material (*f*). Source terms ψ and ϕ in Eqs. (4) and (6) are describing the chemical reaction of hydrogen with the hydride material, see appendix.

Mass balance equation of the hydride bed (G2 in Figure 3):

$$\varepsilon_b \frac{\partial \rho_f}{\partial t} + \nabla \cdot \left(\rho_f \vec{v}_{f,b} \right) = -\psi \tag{4}$$

Darcy's Law for the flow velocity vector in Eqs. (4) and (6):

$$\vec{v}_{f,b} = -\frac{\kappa_b}{\eta_f} \nabla p_b \tag{5}$$

Energy equation of the hydride bed (G2 in Figure3):

$$\left[(1-\varepsilon_b) \left(\rho c_p \right)_s + \varepsilon_b \left(\rho c_p \right)_f \right] \frac{\partial T_b}{\partial t} + \left(\rho c_p \right)_f \vec{v}_{f,b} \nabla T_b = \nabla \cdot \left(k_{eff,b} \nabla T_b \right) + \phi \tag{6}$$

The energy released by the hydride bed during hydrogen absorption is crucial for the thermal design because it has to be removed. The released energy is given by the source term ϕ in Eq. (6). The structure of the source term depends on the applied hydride material, see appendix for sodium alanate.

Energy equation of the reactor element shell tube (G3 in Figure 3):

$$\left(\rho c_p \right)_W \frac{\partial T_W}{\partial t} = \nabla \cdot \left(k_W \nabla T_W \right) \tag{7}$$

Energy equation of the domain of the flowing heat transfer fluid (G4 in Figure 3):

$$\left(\rho c_p \right)_{HTF} \frac{\partial \overline{T}_{HTF}}{\partial t} + \left(\rho c_p \right)_{HTF} \overline{u}_{HTF} \frac{\partial \overline{T}_{HTF}}{\partial z} = \frac{A_0 / L}{A_{q,HTF}} h \left(T_{W,R6} - \overline{T}_{HTF} \right) \tag{8}$$

In the mathematical model heat transfer from the outer surface of the reactor element shell tube to the heat transfer fluid appears as the source term of Eq. 8, containing the heat transfer coefficient *h*. Correlations of heat transfer coefficients *h* are given in [7] and [8].The direction of the spatial *z*-coordinate in the flow direction of the heat transfer fluid is illustrated in Figure 2.

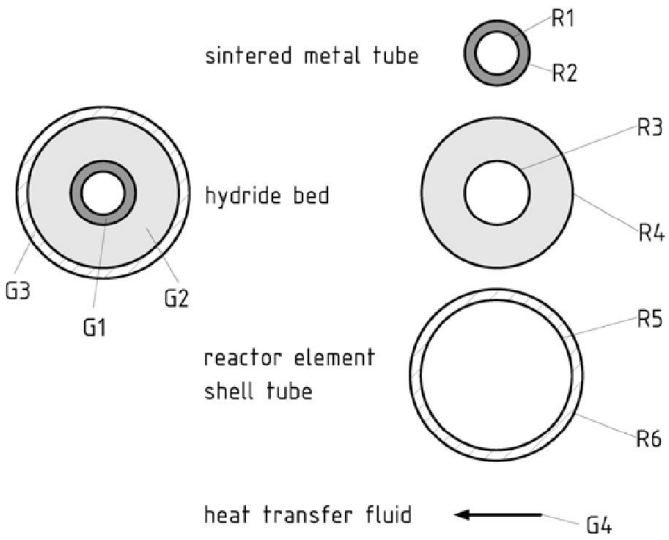

Figure 3 Calculation domains (G1 – G4) and their boundaries (R1 – R6) of the mathematical model.

Boundary conditions

To describe a specific process the balance equations must be completed by boundary and initial conditions. Figure 3 reveals that each domain (G1- G3) has two boundaries (R1 – R6). With respect to the whole reactor element R1 and R6 are exterior boundaries, while the calculation domains are coupled by interior boundaries R2 – R5. Domains G1 and G2 are coupled where R2 und R3 coincide, and G2 and G3 where R4 and R5 coincide, respectively (Figure 3).

If the loading pressure of the storage tank is given, the boundary condition (R1) of Eq. (2) becomes:

$$p_t \big|_{R1} = p_{H_2}(t) \,. \tag{9}$$

During desorption R1 is an outlet of hydrogen. The applied desorption pressure, Eq. (9), or mass flux to a fuel cell, Eq. (10), can be chosen as boundary conditions.

$$-\vec{n}\left(\rho_f \vec{v}_f\right)_{t,R1} = -\vec{n}\left(\rho_f \vec{v}_f\right)_{out} \tag{10}$$

With respect to energy transport boundary R1 is a discontinuity [9]. On the side of hydrogen supply from the refueling station there is only convective transport, i.e. an enthalpy flow of hydrogen is entering the boundary R1 in case of absorption. Just behind the boundary on the side of the sintered metal there are immediately two mechanisms of energy transport: Firstly there is still convective transport by hydrogen flow and additionally effective heat conduction ($k_{eff,t}$) of the porous medium, Eq. 6. An enthalpy flow and a heat flux are leaving the boundary R1. Because of conservation of energy there must be a jump of enthalpy flow represented by a sudden change of hydrogen temperature from $T_{H2,in}$ to $T_t|_{R1}$. Equation (11) is the boundary condition of energy equation (6) in case of hydrogen absorption.

$$-k_{eff,t}\left.\frac{\partial T_t}{\partial n_v}\right|_{R1} + \left(\rho c_p\right)_f v_{f,t_n} T_t\big|_{R1} = \left(\rho c_p\right)_f v_{f,in} T_{H_2,in} \tag{11}$$

In case of desorption corresponding considerations lead to boundary condition (12) for energy equation (6). Taking into account the Second Law of Thermodynamics the temperature profile must have a horizontal tangent [10,11].

$$-k_{eff,t}\left.\frac{\partial T_t}{\partial n_v}\right|_{R1} = 0 \tag{12}$$

Boundary conditions of the type of Eqs. (11) and (12) have been originally applied to mass transfer problems with dispersion phenomena [10] and later extended to describe axial dispersion effects in heat exchangers [11,12]. Due to their origin these boundary conditions are called Danckwerts conditions.

At the coupling between sintered metal tube (G1) and hydride bed (G2) the mass flux through coinciding boundaries R2 und R3 remains constant, yielding boundary condition (13) for mass balance equations (1) and (4).

$$-\vec{n}\left[\left(\rho_f \vec{v}_f\right)_{t,R23} - \left(\rho_f \vec{v}_f\right)_{b,R23}\right] = 0 \tag{13}$$

Application of the first law of Thermodynamics to boundaries R2 and R3 coupling G1 and G2 (Figure 3) yields the general form of the boundary conditions for energy equations (3) and (6):

$$\begin{aligned} &-k_{eff,t}\left.\frac{\partial T_t}{\partial n_v}\right|_{R23} + \left(\rho c_p\right)_f v_{f,n} T_t\big|_{R23} \\ &= -k_{eff,b}\left.\frac{\partial T_b}{\partial n_v}\right|_{R23} + \left(\rho c_p\right)_f v_{f,n} T_b\big|_{R23} \end{aligned} \tag{14}$$

In case of ideal thermal contact between sintered metal tube (G1) and hydride bed (G2) boundary condition (14) reduces to:

$$-k_{eff,t}\left.\frac{\partial T_t}{\partial n_v}\right|_{R23} = -k_{eff,b}\left.\frac{\partial T_b}{\partial n_v}\right|_{R23} . \tag{15}$$

Since the wall of the reactor element shell tube (G3) is impermeable for hydrogen the boundary condition of mass balance equation (4) at boundary R4 is no-flux condition (16).

$$-\vec{n}\left(\rho_f \vec{v}_f\right)_{b,R4} = 0 \tag{16}$$

Assuming ideal thermal contact between hydride bed (G2) and reactor element shell tube (G3) the boundary condition (17) holds for energy equations (6) and (7) at R4 and R5, respectively.

$$T_b\big|_{R45} = T_W\big|_{R45} \tag{17}$$

At the outer boundary R6 of the reactor element heat is transferred to the heat transfer fluid, yielding boundary condition (18) for energy equation (7).

$$-k_W\left.\frac{\partial T_W}{\partial n}\right|_{R6} = h\left(T_{W,R6} - \overline{T}_{HTF}\right) \tag{18}$$

The energy equation of the heat transfer fluid (8) requires one inlet condition only, which is the inlet temperature of the heat transfer fluid:

$$\overline{T}_{HTF}(z=0) = T_{HTF,in} \tag{19}$$

Initial conditions

Initial conditions have to be set for T_t, p_t, T_b, p_b, T_W, T_{HTF}, X_β and X_γ, representing e.g. the state of the empty tank arriving at the refueling station. The initial density of hydrogen ρ_f, Eqs. (1) and (4), results from the thermal equation of state, i.e. the ideal gas law in this model.

SODIUM ALANATE AS ACTIVE HYDRIDE MATERIAL

Due to the latest developments on the field of light metal hydride sodium alanate has been specified as the active material in STORHY [1]. This material is especially promising because of its high theoretical hydrogen capacity of 5.6 % and the feasibility of large-scale synthesis [13,14]. The practical hydrogen capacity strongly depends on the synthesis method of the storage material and the applied catalyst. The effective kinetic is continuously improved during the project while the practical hydrogen capacity is varying between 3.5 % and 4.85 % [14].

Table 1 shows the characteristics of the reversible chemical reaction between the active material and hydrogen. Starting point is an equimolar mixture of sodium hydride and aluminum. This mixture contains additional catalysts and compounds enhancing the effective thermal diffusivity of the hydride bed [14 - 16]. The total reaction consists of two steps,

Table 1. In this work the reaction steps are denoted with β and γ, respectively. Considering hydrogen absorption, in the first reaction step β, the complete amount of sodium hydride reacts with a portion of the initially provided aluminum and hydrogen to the intermediate product Na_3AlH_6. In the second step γ this intermediate product reacts with further hydrogen and the remaining aluminum to sodium alanate. The absorption reaction of hydrogen is exothermic, the desorption reaction of hydrogen is endothermic. The total enthalpy of reaction is 40 kJ per mole hydrogen.

Table 1 Characteristics of sodium alanate: total reaction and reaction steps

	chemical reaction equation	ΔH_R	w
		[kJ/mol]	[%]
total reaction	3 NaH + 3 Al + 9/2 H_2 ⇌ 3 $NaAlH_4$	40	4.85
reaction step β	3 NaH + Al + 3/2 H_2 ⇌ Na_3AlH_6	49	1.85
reaction step γ	Na_3AlH_6 + 2 Al +3 H_2 ⇌ 3 $NaAlH_4$	33	3.00

REFUELING CRITERIA

The hydrogen content w is commonly used to describe refueling processes of hydride materials. This time-dependent quantity is the ratio between absorbed mass of hydrogen to the initial mass of active material, Eq. (20).

$$w = \frac{m_{H_2}}{m_{Me}^0} = \frac{m_{H_2}}{m_{NaH}^0 + m_{Al}^0} \tag{20}$$

The maximum hydrogen content depends on the hydride material, its manufacturing process and kind and amount of additional compounds.

$$w_{\max} = \frac{m_{H_2}^{\max}}{m_{Me}^0} = \frac{m_{H_2}^{\max}}{m_{NaH}^0 + m_{Al}^0} \tag{21}$$

The criterion of fast filling is formulated applying the normalized hydrogen content X. This is the ratio of actual hydrogen content w to the maximum hydrogen content $w_{\max}$. Equation (22) clarifies that the normalized hydrogen content is the ratio of actually absorbed mass of hydrogen to the maximally absorbable mass of hydrogen.

$$X = \frac{w}{w_{\max}} = \frac{m_{H_2}}{m_{Me}^0}\frac{m_{Me}^0}{m_{H_2}^{\max}} = \frac{m_{H_2}}{m_{H_2}^{\max}} \tag{22}$$

Table 2 Criterion of fast refueling in EU project STORHY

	t	X
	[s]	[-]
first sub-criterion	600	0.80
second sub-criterion	1000	0.98

The criterion of fast refueling is fulfilled if the storage tank is loaded to 80 % after 600 s and nearly to 100 % after 1000 s, Table 2.

SIMULATION RESULTS

The influence of the flow rate of the heat transfer fluid on the absorption behavior of the storage tank is investigated by simulating three operating conditions of the storage tank (I – III) with different flow rates. The remaining parameters are equal for all considered operating conditions: The initial temperature of the storage tank is 100 °C and initially the storage tank contains no hydrogen. The constant loading pressure is 100 bar and the constant inlet temperature of the heat transfer fluid is 100 °C. The heat transfer coefficient between the outer surfaces of the reactor element shell tubes und the heat transfer fluid is calculated by empirical correlations as a function of the flow rate of the heat transfer fluid [7,8], Table 3.

Table 3 Simulated operating conditions of the manufactured storage tank

operating condition	$\dot{V}_{HTF}$	h	$\bar{u}_{HTF}$
	[m^3/h]	[W/(m^2 K)]	[m/s]
I	12	420	0.25
II	6	218	0.12
III	3	102	0.06

Subsequently it is investigated how heat transfer enhancement - e.g. by additional flow baffles - influences the absorption behavior. For this purpose the heat transfer coefficient is systematically varied for a selected fixed flow rate. The theoretical limit is an infinite heat transfer coefficient, i.e. surface temperature and temperature of the heat transfer fluid are identical, Table 4.

Table 4 Heat transfer enhancement between surface of reactor element shell tubes and heat transfer fluid

	$\dot{V}_{HTF}$	h
	[m^3/h]	[W/(m^2 K)]
reference state	12	420
additional flow baffles	12	2000
theoretical limit	12	$\rightarrow\infty$

Figure 4 shows the normalized hydrogen content as a function of time for three different flow rates of the heat transfer fluid. The operating conditions I and II fulfill the criteria of fast refueling (Table 5), while operating condition III does not. With respect to the manufactured storage tank the flow rate of the heat transfer fluid must be sufficiently high to fulfill the criteria of fast refueling. Thereby it is crucial that the heat transfer coefficient between reactor element shell tube and heat transfer fluid strongly increases with increasing flow rate of the heat transfer fluid because of increasing mean flow velocities, Table 3. The heat capacity rate of the heat transfer fluid itself is of secondary importance under the considered circumstances.

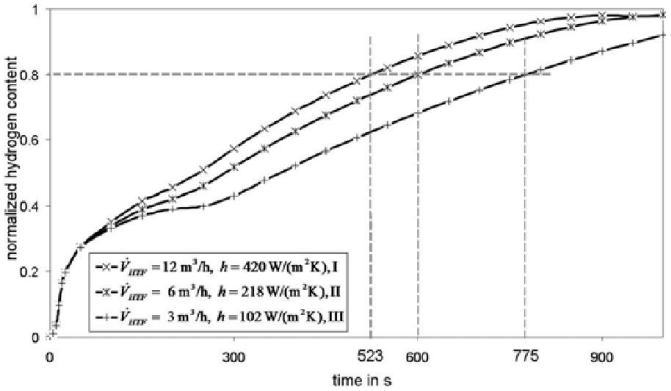

Figure 4 Absorption behavior for operating conditions I, II and III

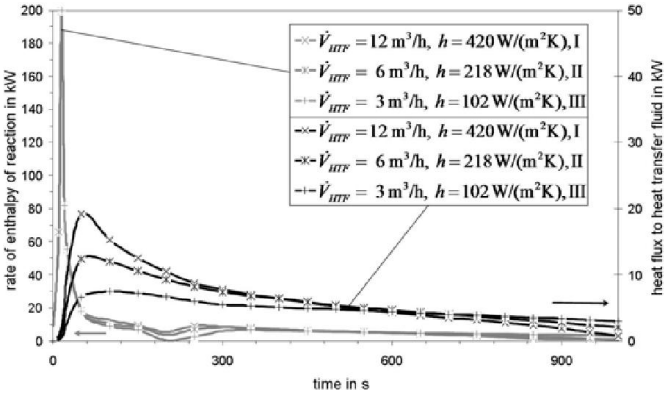

Figure 5 Rate of enthalpy of reaction and heat flux to the heat transfer fluid for operating conditions I, II and III

Table 5: Fulfillment of the criteria of fast refueling

operating condition	X (t = 1000 s)	t (X = 0.8)	criteria of Table 2
	[-]	[s]	
I	0.98	523	fulfilled
II	0.98	600	fulfilled
III	0.95	775	not fulfilled

During the first 75 s the absorption curves I - III are nearly identical (Figure 4), i.e. the influence of the flow rate of the heat transfer fluid on the absorption behavior is negligible. Later on the influence of different flow rates becomes significant. The resulting loading times are given in Table 5. Figure 5 clarifies the coupling between thermal and absorption behavior of the process. At the beginning the heat flux to the heat transfer fluid is small compared to the rate of enthalpy of reaction. Because of the large heat capacities of the system most of the released chemical energy is intermediately stored in the hydride bed, the sintered metal tube and the reactor element shell tubes, respectively. The temperature of the storage tank and the inflowing hydrogen rises and only a small amount of heat is transferred to the heat transfer fluid. The rate of enthalpy of reaction is a direct measure for the mass flow rate of absorbed hydrogen. At the beginning of the absorption process the rate of enthalpy of reaction is equal for all three operating conditions, Figure 5. At t = 15 s the peak value is 200 kW. Already after 50 s the rates of enthalpy of reaction are below 20 kW.

An additional important characteristic is an intermediate slow-down of the process which becomes apparent by the declining slope of the absorption curves (Figure 4). Afterwards the process accelerates again. This effect is most distinct for operating condition III. The process slows down after the first 75 s because the first reaction step comes to completion. Due to the temperature field of the hydride bed the end of the first reaction steps is shifted in time depending on the local position of the hydride bed, resulting in a continuous slow-down and not a sharp ending. The second reaction step cannot start immediately after the first reaction step because the temperatures of the hydride bed are too high, see Table A1 (appendix). Therefore, the first reaction step is followed by a cooling phase with no reaction where the driving pressure difference for the second reaction step develops with decreasing temperature of the hydride bed. Since there is a temperature field the reaction starts shifted in time depending on the local position and nearly runs to completion within the considered time interval of 1000 s, Table 5. The slow-down of the absorption process becomes apparent by the minima of the rate of enthalpy of reaction, Figure 5 and Table 6. For operating condition III the absorption process practically stops at t = 193 s where the rate of enthalpy of reaction is only 0.5 kW.

Table 6 Slow-down of absorption process between first and second reaction step

$\dot{V}_{HTF}$	minimum rate of enthalpy of reaction	time
[m³/h]	[kW]	[s]
12	4.9	178
6	3.6	186
3	0.5	193

The largest heat flux from the reactor element shell tubes to the heat transfer fluid of 19.2 kW occurs in operating condition I, Figure 5. This heat flux is well below the maximum rate of enthalpy of reaction of 200 kW confirming the strong influence of the heat capacities of the system on the absorption behavior. Since the energy released during the chemical reaction is mainly stored as internal energy due to the large heat capacities and transferred to the heat transfer fluid with a time delay the heat fluxes to the heat transfer fluid are relatively small during the whole absorption process for all three operating conditions (Figure 5). This explains the relatively small increase of the temperature of the heat transfer fluid inside the storage tank, Table 7.

Table 7 Maximum heat flux to heat transfer fluid and maximum outlet temperature of the heat transfer fluid

$\dot{V}_{HTF}$	maximum heat flux	time	maximum outlet temperature	time
[m³/h]	[kW]	[s]	[°C]	[s]
12	19.2	47	104	51
6	12.9	62	105	68
3	7.5	83	106	109

For the design flow rate of the storage tank (12 m^3/h) the effect of additional measures of enhanced heat transfer on the performance of the storage tank are investigated, e.g. installation of flow baffles within the tube-bundle. The longitudinal flow apparatus becomes a shell-and-tube apparatus with flow baffles. Because of the cross flow of the shell-side heat transfer fluid over the tubes the heat transfer coefficients are larger compared to longitudinal flow. The modified design requires additional passive masses. However, passive masses have to be minimized for mobile applications. Their implementation is only justified if there are significant advantages with respect to fast refueling. As reference the manufactured longitudinal flow shell and tube apparatus with operating condition I, Table 3, is chosen. Figure 6 shows the effects of enhanced heat transfer from the outer surface of the reactor element shell tubes to the heat transfer fluid for a flow rate of the heat transfer fluid of 12 m^3/h.

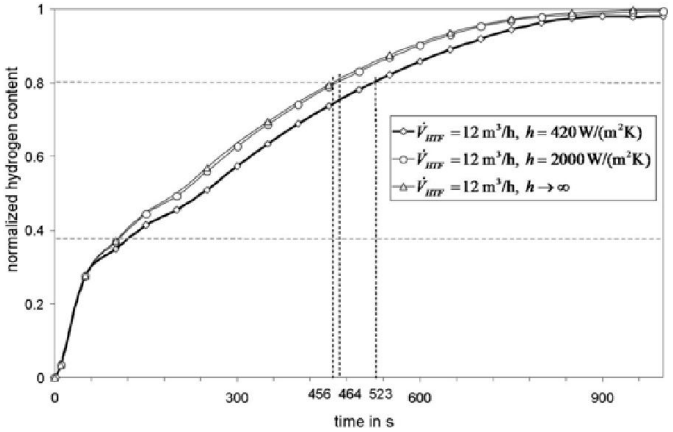

Figure 6 Enhancement of heat transfer between outer surface of reactor element shell tubes and heat transfer fluid

An increase of the heat transfer coefficient from 420 W/(m^2 K) to 2000 W/(m^2 K) shortens the absorption process by 1 minute. Further increase of the heat transfer coefficient to the upper limit at which wall temperature and temperature of the heat transfer fluid are identical shortens the absorption process by further 8 s. Heat transfer enhancement on the side of the heat transfer fluid has no influence on the absorption behavior at the beginning of the process. The temperature field of the hydride bed and therefore its absorption behavior are determined by the heat capacities of the system. As observed in Figure 4 and Figure 5 heat transfer to the heat transfer fluid influences the absorption behavior only at later times, i.e. $t > 75$ s.

CONCLUSIONS

The flow rate of the heat transfer fluid is decisive for fast refueling. With volumetric flow rate of 6 m^3/h the criterion of loading up to 80 % in 600 s is exactly fulfilled. If the flow rate is too low, neither the criterion of loading up to 98 % in 1000 s nor the criterion of loading up to 80 % in 600 s can be fulfilled. At the beginning of the absorption process the flow rate of the heat transfer medium plays a secondary role. The released energy of the chemical reaction is stored as internal energy due to the heat capacities of the masses of the storage tank and the hydrogen flow entering the reactor elements with ambient temperature. This effect is especially important for sodium alanate tanks. Because of the high loading pressure (100 bar) the wall thickness of the reactor element shell tubes is high resulting in large masses and heat capacities of the system. Enhanced heat transfer by additional flow baffles does not shorten the refueling process in such a degree that its realization seems so to be justified, especially in case of automotive applications.

APPENDIX: EQUILIBRIUM AND KINETICS DATA OF SODIUM ALANATE

Source term of mass balance equation (4):

$$\psi = \rho_s \left(1-\varepsilon_b\right)\left[w_\beta^{\max}\dot{X}_\beta + w_\gamma^{\max}\dot{X}_\gamma\right] \tag{23}$$

Source term of energy equation (6):

$$\phi = \rho_s \left(1-\varepsilon_b\right)\frac{1}{M_{H_2}}\left[w_\beta^{\max}\left|\dot{X}_\beta\right|\Delta H_R^\beta + w_\gamma^{\max}\left|\dot{X}_\gamma\right|\Delta H_R^\gamma\right] \tag{24}$$

Reaction kinetics of sodium alanate expressed as rate of change of the normalized hydrogen content for both reaction steps are given by Eqs. (25) – (30) [17]. Equations (25) – (27) refer to the first reaction step of absorption (β), and Eqs. (28) – (30) to the second step (γ).

$$\dot{X}_{\beta,1} = 28\cdot 10^{10}\,\frac{1}{\mathrm{s}}\exp\left(\frac{-117517\,\frac{\mathrm{J}}{\mathrm{mol\,K}}}{RT}\right)\left(1-X_\beta\right)\left[-\ln\left(1-X_\beta\right)\right]^{0.286} \tag{25}$$
$$\left(\frac{p-p_{eq,\beta}}{p_{eq,\beta}}\right)$$

$$\dot{X}_{\beta,2} = 128928\cdot 10^{3}\,\frac{1}{\mathrm{s}}\exp\left(\frac{-86446\,\frac{\mathrm{J}}{\mathrm{mol\,K}}}{RT}\right)\left(1-X_\beta\right) \tag{26}$$
$$\left(\frac{p-p_{eq,\beta}}{p}\right)$$

$$\dot{X}_\beta = \min\left[\dot{X}_{\beta,1};\dot{X}_{\beta,2}\right] \tag{27}$$

$$\dot{X}_{\gamma,1} = 0.5166\,\frac{1}{\mathrm{s}}\exp\left(\frac{-54660\,\frac{\mathrm{J}}{\mathrm{mol\,K}}}{RT}\right)X_\beta\left(1-X_\gamma\right)\left[-\ln\left(1-X_\gamma\right)\right]^{0.286} \tag{28}$$
$$\ln\left(\frac{p}{p_{eq,\gamma}}\right)\left(\frac{p}{p_0}\right)^{2.7}$$

$$\dot{X}_{\gamma,2} = 1874.7\frac{1}{\mathrm{s}}\exp\left(\frac{-62933\frac{\mathrm{J}}{\mathrm{mol\,K}}}{RT}\right)X_{\beta}\left(1-X_{\gamma}\right)\ln\left(\frac{p}{p_{eq,\gamma}}\right)\left(\frac{p}{p_0}\right)^{1.5} \quad (29)$$

$$\dot{X}_{\gamma} = \min\left[\dot{X}_{\gamma,1};\dot{X}_{\gamma,2}\right] \quad (30)$$

Equilibrium data of the sodium alanate–hydrogen–system, Eqs. (31) and (32), are required for obtaining the driving force of the chemical reaction ($p > p_{eq}$ for absorption) in Eqs. (25), (26), (28) and (29) [17]:

$$\ln\left(\frac{p_{eq,\beta}}{p_0}\right) = \frac{-49014\frac{\mathrm{J}}{\mathrm{mol}}}{RT} - \frac{-130.21\frac{\mathrm{J}}{\mathrm{mol\,K}}}{R} \quad (31)$$

$$\ln\left(\frac{p_{eq,\gamma}}{p_0}\right) = \frac{-33096\frac{\mathrm{J}}{\mathrm{mol}}}{RT} - \frac{-113.72\frac{\mathrm{J}}{\mathrm{mol\,K}}}{R} \quad (32)$$

Table A1 Equilibrium data required for the consideration of loading process with 100 bar, calculated form Eqs. (31) and (32). For loading an alanate storage tank the necessary condition is $p > p_{eq}$.

T	ϑ	$p_{eq,\beta}$	$p_{eq,\gamma}$
[K]	[°C]	[bar]	[bar]
439	166	9.25	**100**
533	260	**100**	498

REFERENCES

[1] StorHy (Hydrogen Storage Systems for Automotive Application), URL: < www.storhy.net >, *Integrated Project within the EU 6th Framework Programme coordinated by MAGNA STEYR Fahrzeugtechnik AG & Co KG (2004-2008)*, 2008

[2] Na Ranong, C., Höhne, M., Franzen, J., Hapke, J., Fieg, G., Dornheim, M., Eigen, N., von Colbe, J.M.B. and Metz, O., Concept, Design and Manufacture of a Prototype Hydrogen Storage Tank Based on Sodium Alanate, *Chemical Engineering & Technology*, Vol. 32, 2009, pp. 1154-1163

[3] Wagner, W., Wärmeträgertechnik mit organischen Fluiden. Würzburg: Vogel, 2005

[4] AD 2000-Regelwerk. Köln: Heymanns, 2000

[5] COMSOL Multiphysics Version 3.4, Computer Software, COMSOL AB, Copyright 1994-2007. Zoetermeer: Comsol, 2007

[6] Nield, D.A. and Bejan, A., Convection in Porous Media. New York: Springer, 2006

[7] VDI-Wärmeatlas : Berechnungsunterlagen für Druckverlust, Wärme- und Stoffübergang. Berlin: Springer, 2006

[8] Schneider, S., Untersuchungen zum lokalen Wärmeübergangsverhalten im Längsstrom-Rohrbündelwärmeübertrager mit geschlitzten Stützblechen. Düsseldorf: VDI, 1997

[9] Müller, I., Grundzüge der Thermodynamik mit historischen Anmerkungen. Berlin: Springer, 2001

[10] Danckwerts, P.V., Continuous Flow Systems : Distribution of Residence times, *Chemical Engineering Science*, Vol. 2, 1953, pp. 1-13

[11] Luo, X. and Roetzel, W., Extended Axial Dispersion Model for Transient Analysis of Heat Exchangers, *4th UK National Conference on Heat Transfer*, Vol. 1995, 1995, pp. 411-416

[12] Roetzel, W. and Na Ranong, C., Consideration of Maldistribution in Heat Exchangers Using the Hyperbolic Dispersion Model, *Chemical Engineering and Processing*, Vol. 38, 1999, pp. 675-681

[13] Eigen, N., Keller, C., Dornheim, M., Klassen, T. and Bormann, R., Industrial Production of Light Metal Hydrides for Hydrogen Storage, *Scripta Materialia*, Vol. 56, 2007, pp. 847-851

[14] Eigen, N., Gosch, F., Dornheim, A., Klassen, T. and Bormann, R., Improved Hydrogen Sorption of Sodium Alanate by Optimized Processing, *Journal of Alloys and Compounds*, Vol. 465, 2008, pp. 310-316

[15] Fichtner, M., Engel, J., Fuhr, O., Kircher, O. and Rubner, O., Nanocrystalline Aluminium Hydrides for Hydrogen Storage, *Materials Science and Engineering B-Solid State Materials for Advanced Technology*, Vol. 108, 2004, pp. 42-47

[16] Bogdanovic, B., Felderhoff, M., Kaskel, S., Pommerin, A., Schlichte, K. and Schuth, F., Improved Hydrogen Storage Properties of Ti-Doped Sodium Alanate Using Titanium Nanoparticles as Doping Agents, *Advanced Materials*, Vol. 15, 2003, pp. 1012-1015

[17] Franzen, J., Modellierung und Simulation eines Wasserstoffspeichers auf der Basis von Natriumalanat. Fortschritt-Berichte VDI: Reihe 6, Energietechnik, 583, Düsseldorf: VDI, 2009